Oleg V. Trifonov[1]
Research Institute for Natural Gases and Gas Technologies (GAZPROM VNIIGAZ),
Razvilka poselok,
Leninsky District,
Moscow 142717, Russia
e-mail: O_Trifonov@vniigaz.gazprom.ru

Vladimir P. Cherniy
Research Institute for Natural Gases and Gas Technologies (GAZPROM VNIIGAZ),
Razvilka poselok,
Leninsky District,
Moscow 142717, Russia

Application of Composite Wraps for Strengthening of Buried Steel Pipelines Crossing Active Faults

In the paper, the efficiency of strengthening of a buried steel pipeline with a composite wrap subjected to an active faults action is analyzed. A three-dimensional numerical model of the pipeline is developed. The pipeline is considered as an elastoplastic steel shell, while the composite wrap is represented as an orthotropic elastic shell. The model takes into account the elastoplastic behavior of soil, contact interaction between the soil and the pipe, large inelastic strains, distortion of the pipeline cross section, and local buckling formation. A normal-slip fault kinematics with large fault offsets is considered in numerical modeling. The effect of the wrap thickness, length, and position relative to the fault plane is analyzed. [DOI: 10.1115/1.4032915]

1 Introduction

Buried steel pipelines crossing active tectonic faults should be designed to withstand predicted fault displacements. Under the fault action, a pipeline is subjected to intense bending and axial loads arising from relative displacements of adjacent soil blocks along the fault plane. The magnitude of soil displacements can reach several meters, and the direction of soil displacements is determined by fault kinematics (strike-slip, normal-slip, etc.). During the past seismic events, pipeline damages and failures due to fault offsets were observed and documented in the papers [1–6]. Typical limit states include tensile failure, local buckling of the pipe wall, and cross-sectional distortion. Failure can also occur in the form of combination of the mentioned mechanisms. Realization of particular failure mechanism depends on a number of factors, including fault kinematics and crossing angle, soil conditions, pipeline geometry and material properties, and action of other loads. However, the importance of possible limit states is different. The serviceability limit states, such as cross-sectional distortion, do not affect the operability of the pipeline, but cause problems for maintenance operations on a pipeline with the use of pigging devices. Tensile failure with integrity loss of the pipeline is the most important limit state often leading to a severe ecological damage. Local buckling of the pipe wall on the early stage does not present a critical threat to the pipeline. But on the final stage with fully developed wrinkles and high strain concentration, the integrity loss can occur especially under varying operational loads (pressure and temperature) in the form of fatigue crack propagation.

The reliability of a pipeline crossing active fault should be verified by a stress–strain analysis under estimated fault displacements. Corresponding stress–strain analysis methods have been developing since 1970s starting from simplified analytical approaches [7,8] followed by more advanced analytical [9–11] and numerical [12–20] techniques.

In the paper [7], the pipeline crossing a strike-slip fault is considered as a cable with only axial deformations accounted for. In the subsequent paper [8], bending strains are also incorporated into the model. In recent analytical work [9–11], the inelastic behavior of a pipeline and tension–bending interaction are taken into account, and different types of fault kinematics are analyzed.

Numerical finite-element models developed over the last decades include beam-type models [12–15] and three-dimensional shell-type models [16–20]. In the former models, the pipe is considered as a beam structure and the pipe–soil interaction is represented by discrete soil springs. In the latter models, the pipeline is considered as a shell structure and the surrounding soil is represented as a continuum medium. In contrast to the beam-type models, the shell-type models directly describe local failure mechanisms (local wall buckling and cross-sectional distortion).

Traditional design measures to prevent pipeline failure at fault crossing include special requirements to the trench backfill materials, trench geometry, and the pipe wall thickness calculation with account for fault loads. Nevertheless, it is almost impossible to ensure reliability of a pipeline with respect to extremely large fault offsets. Under such conditions, serviceability limit states should be admitted. Still, critical limit states corresponding to the integrity loss must be prevented. Taking into account the economical component of the projects, increasing the pipe wall thickness can be effective and reasonable only to some extent. In these circumstances, the use of composite wrappings can be considered as an alternative measure to pipeline strengthening.

Composite sleeves and wraps have been applied over the last 20 years for repair and strengthening purposes. Composite repair systems have shown their effectiveness in strengthening of pipe sections weakened due to corrosion, dents, gouges, and other local defects [21–31]. The effect of strengthening in such systems is achieved by redistribution of the total hoop forces between the pipe wall and the wrap due to substantial rigidity of the fiber-reinforced composite wraps in the hoop direction.

The application of composite wraps for strengthening of long pipeline segments should be preceded by the estimation of its geometrical parameters (sufficient thickness and length) and positioning along the pipe. Correct estimation of these parameters is crucial for an effective reinforcement of the pipeline and prevention of pipe failure under extreme loads. Thus, the methods for stress–strain analysis of the system "pipeline–wrap–soil" taking into account large inelastic deformations should be developed. Until recently, such methods have been lacking.

The application of composite wraps for strengthening of relatively long pipeline segments was first analyzed in the paper [32]. A new analytical model for stress–strain analysis of a wrapped pipe under the action of internal pressure and temperature was developed and verified against test results obtained for a pipe with elliptical end plugs (pressure vessel). The case of a buried steel pipeline under the action of internal pressure and temperature was analyzed in comparison to a finite-element model. It was shown

[1]Corresponding author.

Contributed by the Pressure Vessel and Piping Division of ASME for publication in the Journal of Pressure Vessel Technology. Manuscript received June 10, 2015; final manuscript received March 2, 2016; published online July 18, 2016. Editor: Young W. Kwon.

that composite wrappings can be effectively used as a regular reinforcement on relatively long pipeline segments subjected to the internal pressure and temperature loads. In Ref. [32], it was suggested that the application of composite wraps can be considered as a strengthening measure for pipelines crossing active tectonic faults or laid in other harsh environmental conditions.

In the present article, a buried steel pipeline with a composite wrap at active fault crossing is considered. To analyze the effect of the wrap on mechanical behavior of the pipeline under the fault offset, a three-dimensional numerical finite-element model is developed in Secs. 2 and 3. The model takes into account the material and geometric nonlinearities of the system. In Sec. 4, the numerical results for the case of normal-slip fault action on the pipeline are presented and analyzed. In Sec. 5, a parametric analysis of the wrap length and thickness is performed.

2 Structural Model of the Reinforced Pipeline at the Fault Crossing

Consider a buried steel pipeline crossing a normal-slip fault at a right angle (Fig. 1). The structural model is constructed for a brick-shaped soil volume enclosing the pipeline. To represent the fault action on the pipe, the soil volume is divided into two blocks—the stationary block and the moving block. The fault offset is modeled by the application of vertical displacements Δf to the boundaries of the moving block. A composite wrap is applied to the part of the pipeline in the vicinity of the fault plane. The lengths of the reinforced pipe segments on the stationary and moving blocks are designated as L_{w1} and L_{w2} correspondingly. The dimensions of the model are listed in Table 1.

The size of the finite-element model is a substantial factor affecting the calculation time, especially when a parametric study is to be performed. Accordingly, the dimensions of the soil domain were taken based on a compromise between the minimization of the effects of boundaries and acceptable computational time. For the adopted domain dimensions, the effect of the boundaries was found to have minor influence on stress–strain state of the pipeline under considered fault offsets. This factor does not affect the results and conclusions of the performed analysis. For example, comparing the results for the depth parameter $W_2 = 4$ m and 8 m, it was found that the difference in maximal compressive strains in the pipeline under the fault offset of 3 m did not exceed 6%.

Maximal fault offset considered in simulation was equal to 3.0 m. The wrap thickness t_w was set in the range of 5–30 mm. The lengths of the reinforced pipe segments L_{w1} and L_{w2} were set in the range of 4.5–28.5 m.

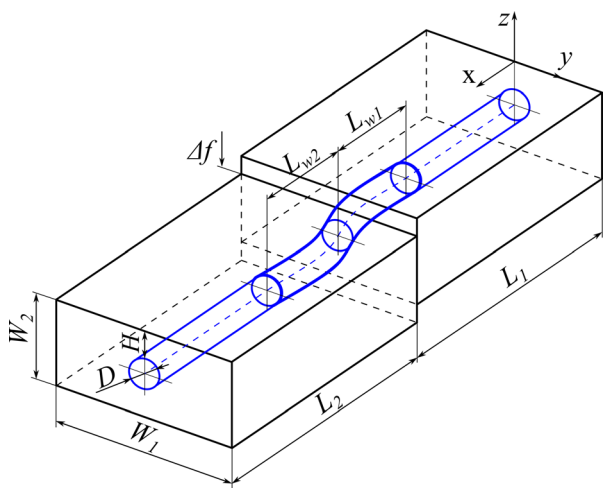

Fig. 1 Structural model of a reinforced pipe crossing a normal-slip fault

Table 1 Geometrical dimensions of the structural model

L_1 (m)	L_2 (m)	W_1 (m)	W_2 (m)	H (m)	D, mm (in.)	t (mm)
30	30	12	4	1.0	1020 (40)	13.9

The pipeline is considered as a cylindrical shell within the Reissner–Mindlin shell theory with account for shear deformations [33,34]. The pipeline material is taken as the API 5L X60 steel with the Young's modulus of $E_s = 206$ GPa, the Poisson's ratio of $\nu = 0.3$, and the yield stress of $\sigma_Y = 415$ MPa. The stress–strain curve is approximated by the Ramberg–Osgood relations [35] $\varepsilon = \sigma/E + K \cdot (\sigma/E)^n$ with the parameters $n = 15.45$ and $K = 13.76 \times 10^{38}$. This curve is used in the finite-element analysis within the von Mises plasticity material model with nonlinear isotropic hardening. The yield criterion is given by the relation [36]

$$\sigma_e - \sigma_y(W_p) = 0 \tag{1}$$

where σ_e is the equivalent stress and $\sigma_y(W_p)$ is the variable yield stress depending on the value of the plastic work W_p.

The wrap consists of several reinforcing layers of biaxial woven glass fiber fabric and a polymeric epoxy matrix. The reinforcing layers are applied consecutively on the preliminary prepared pipe surface by wrapping. Polymeric epoxy resin provides the bond between the layers of the reinforcing material and between the pipe and the composite wrap. Mechanical properties of glass fibers and epoxy result in almost linear elastic behavior of the composition until failure. Thus, elastic material model is an appropriate choice for the wrap representation.

On a macroscopic scale, a layered composite can be treated as a homogeneous orthotropic material (Fig. 2). Given the mechanical properties of the fibers, matrix, and weave geometry, the elastic constants of the equivalent orthotropic material can be obtained using the approaches of mechanics of composites [37–42]. Assume that principal material directions of each reinforcing layer coincide with the hoop and axial directions of the shell. Then, the principal material axes of the equivalent orthotropic material will be oriented in the hoop, axial, and radial directions (denoted as 1, 2, and 3 in Fig. 2).

Considering a perfect bond between the pipe and the composite wrap, the latter can be represented as an additional layer of the shell structure with orthotropic material properties. In numerical modeling, the following set of elastic constants was used for the orthotropic material representing the wrap [42,43].

The listed constants were determined for a plain weave E-glass fabric/epoxy composite using micromechanical models based on the representative volume cell approach. The obtained results generally correspond to other results obtained for glass/epoxy woven-fiber composites [41]. Such materials are typical for applications considered in the present paper. The elastic moduli in axial and hoop directions in Table 2 are also close to the experimentally determined value (20.4 GPa) of the elastic modulus in the hoop direction for the composite wrap in the paper [32].

In a more detailed analysis, various contact conditions between the pipe and the wrap can be considered, including separation of bonded contact, delamination, frictional sliding, etc. In this case, the wrap should be represented as a separate shell structure, and the contact conditions between the pipe and the wrap should be specified.

Modeling of the mechanical behavior of soil medium presents one of the most important aspects of the problem. Soil plastic failure conditions are characterized by a substantial difference in limit stress under tension and compression and a strong influence of mean pressure on the ultimate shear stresses. These aspects of soil behavior are treated within the plasticity theory with special yield criteria, such as the Mohr–Coulomb or Drucker–Prager criterion [36,44]. In principal stress space, the Mohr–Coulomb

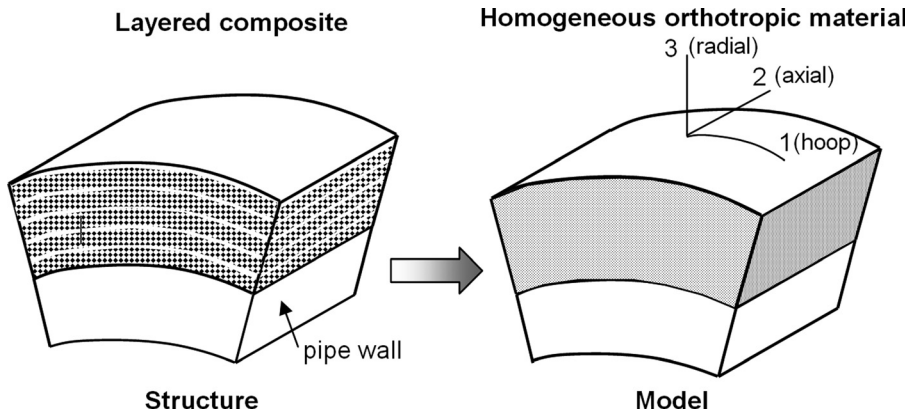

Fig. 2 Schematization of the composite wrap material

Table 2 Mechanical properties of the equivalent homogenized material

E_1 (GPa)	E_2 (GPa)	E_3 (GPa)	G_{12} (GPa)	G_{23} (GPa)	G_{31} (GPa)	ν_{12}	ν_{23}	ν_{31}
18.634	18.634	8.346	3.190	2.422	2.422	0.1745	0.3720	0.3720

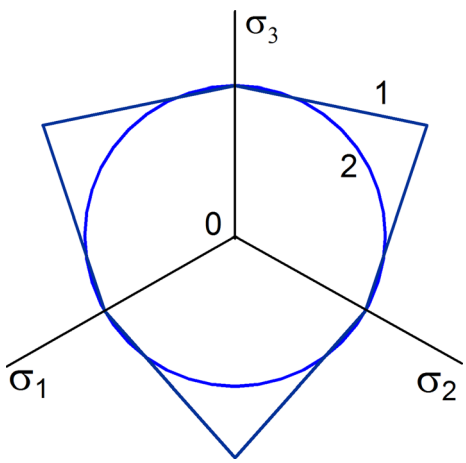

Fig. 3 Deviatoric section of the Mohr–Coulomb and the Drucker–Prager yield surfaces

criterion has the form of a hexagonal cone with the axis of symmetry coinciding with the hydrostatic axis, while the Drucker–Prager criterion yields a circular cone, which can be made to coincide with the inner or outer corners of the Mohr–Coulomb surface.

Another essential property of soils is the dilatancy or plastic change of volume. The dilatancy is described by the angle of dilation ψ defined as the ratio between a volumetric plastic strain rate and a shear strain rate. In the plasticity theory, the effect of dilation is taken into account by replacement of the friction angle ϕ by the dilation angle in the expression for the plastic potential.

In this paper, soil behavior is modeled within the Drucker–Prager plasticity criterion, which can be written in the form

$$\sigma_e + \alpha\sigma_m - \sigma_y = 0 \tag{2}$$

where σ_e is the equivalent stress, σ_m is the mean normal stress, and α and σ_y are the parameters of the criterion calculated according to the relations

$$\alpha = \frac{6\sin\varphi}{3+\sin\varphi} \tag{3}$$

$$\sigma_y = \frac{6c\cos\varphi}{3+\sin\varphi} \tag{4}$$

which define the Drucker–Prager surface coinciding with the inner corners of the Mohr–Coulomb surface. This case is illustrated in Fig. 3 by the deviatoric sections of the Mohr–Coulomb (line 1) and the Drucker–Prager (line 2) yield surfaces.

It is considered that the pipeline is buried in dense sand with numerical values of the material parameters given in Table 3.

The adopted value of the Young's modulus is equal to its value at the depth of the pipe centerline in the initial state, calculated according to the relation suggested in Ref. [45] on the basis of processing of full-scale pipeline test results. Preliminary numerical simulation has shown that the influence of the variability with depth of the Young's modulus on the stress–strain state of the pipeline under the fault action is insignificant.

The values of the friction angle and the dilation angle were derived from the direct shear tests data for dense sand given in Refs. [46] and [47] according to the following steps:

(1) The parameters were transformed from the direct shear to plane strain conditions according to the relations proposed by Davis [48].
(2) Taking into account that in the process of soil inelastic deformation, friction and dilation angles continuously change from their peak values φ_p and ψ_p to residual critical state values φ_{cr} and $\psi_{cr} = 0$, weighted average values were used as constant parameters of the Drucker–Prager

Table 3 Soil parameters adopted in numerical simulation

Unit weight, γ (kN/m^3)	Young's modulus, E_g (MPa)	Cohesion, c (Pa)	Friction angle, ϕ (deg)	Dilation angle, ψ (deg)
17.7	14.8	100	40.7	4.0

plasticity model: $\varphi = \eta \cdot \varphi_p + (1-\eta) \cdot \varphi_{cr}$, $\psi = \eta \cdot \psi_p$ with the weighting parameter η equals 0.25. The value of the weighting parameter was determined as a result of calibration of the Drucker–Prager plasticity model to the experimental results given in Ref. [47].

The pipeline–soil interaction in the developed model is considered as a contact problem. Contact friction is implemented within the Coulomb friction model with the friction coefficient $\mu = 0.3$. This value corresponds to the interface angle of friction equal to $\varphi/2$.

3 Finite-Element Implementation

The developed numerical model is implemented in the finite-element package ANSYS 14.0 [49]. A higher order 3D 20-node solid element SOLID186, supporting the Drucker–Prager plasticity, large deflections, and large strains, was used to mesh the soil volume. A nonuniform finite-element mesh with element concentration in highly stressed regions surrounding the pipe is constructed. Soil element size is also refined in the longitudinal direction in the near-fault zone.

The pipeline was meshed using quadrilateral four-node element SHELL181, which is well suited for modeling of thin to moderately thick shell structures in large displacement and strain analysis. This element can be used for modeling of layered composite or sandwich shell structures. For layered applications, different material properties can be assigned for each layer. Options are available for specifying the thickness, material, orientation, and the number of integration points through the thickness of the layers. In the process of solution, the data corresponding to the stress–strain state of each layer are stored and are used in calculation of the stress resultants of the element. According to the kinematical parameters calculated for the entire element based on its nodal displacements and rotations, the stress–strain evolution of each layer is performed in accordance with prescribed material laws.

The shell-element mesh geometry is defined to adequately represent the limit state of local buckling, which can take place in the highly stressed parts of the pipeline near the fault crossing. The numerical analyses performed in Refs. [17–20] for strike-slip fault crossings have shown that the most significant stresses and plastic strains in the buried steel pipeline are localized on the length of approximately $10D$ along the pipeline on either side of the fault. Still, for normal-slip fault, the lengths of highly stressed segments of the pipeline can be different on stationary and moving sides of the fault due to different soil resistance to upward and downward pipe movement. Accordingly, on the basis of preliminary numerical modeling, the length of the highly stressed zones was assessed as 10.5 m (on the stationary side) and 20 m (on the moving side of the fault). In these zones, the shell-element size was taken equal to $0.065D$ in the hoop and $0.04D$ in the longitudinal directions. Parametric study performed on the stage of development of the present numerical model has shown that the adopted value of the shell-element size gives reasonable accuracy in modeling of the local buckling phenomena. The adopted mesh size parameters are analogous to those taken in Refs. [17–20].

On other parts of the pipeline, a coarser mesh in longitudinal direction was adopted.

The wrap reinforcement is applied within the highly stressed zones of the pipeline. It is defined as a second layer of the shell elements with orthotropic material properties given in Table 2. It is worth noting that the transition from the reinforced part of the pipe to the regular pipe can also present a problematic area under the action of bending stresses due to abrupt change in shell stiffness. Possible stress and strain concentration in these areas should be carefully studied.

The vertical symmetric section of the finite-element model in the deformed state is shown in Fig. 4. In the figure, the central part of the model is depicted.

The interaction between the pipe and the surrounding soil is defined as a surface-to-surface contact using appropriate contact elements and contact algorithms in ANSYS.

The interaction between the soil blocks is implemented within the approach developed in Refs. [19] and [20]. To specify the interaction of the soil blocks along the fault plane, nonlinear spring elements connecting the opposite nodes of the soil blocks are defined. The character of the interaction of the soil blocks is accounted for by the assignment of appropriate stiffness parameters to spring elements in normal and tangential directions. In the present paper, only normal stiffness of the spring elements is set, which corresponds to frictionless relative motion of the soil blocks. In numerical implementation, the distance between the blocks is taken equal to 25 cm in accordance with Ref. [20].

The following boundary conditions were applied on the soil-domain boundaries. The side and bottom surfaces of the soil blocks were constrained in transverse (y) and axial (x) directions; the front and back surfaces (in the yz-plane) were constrained in axial direction. To represent the fault movement, vertical fault displacements were prescribed to the bottom surface nodes of the moving block, while the bottom surface of the stationary block was constrained in vertical (z) direction.

It is to be stressed that the constraints listed above are applied only to the soil elements' nodes. No constraints are applied on the shell-element nodes. Thus, the pipeline is not constrained on its ends. The interaction of the pipeline with the surrounding soil is defined within the contact model.

Considering the intersection of the pipeline with the fault plane at the right angle, the symmetry conditions about the vertical plane passing through the pipe centerline were used to reduce computational time.

4 Numerical Results

In this section, numerical results for specific case of the wrap parameters $t_w = 15$ mm, $L_{w1} = 10.5$ m, and $L_{w2} = 7.5$ m are presented and discussed in comparison to numerical results for an unreinforced pipeline. Besides the fault offset, the pipeline is subjected to the internal pressure of 7.4 MPa and soil gravity load.

The loads are applied in several steps. Gravity load and the internal pressure are applied on the first step, while monotonically increasing fault displacements are applied on subsequent loading steps.

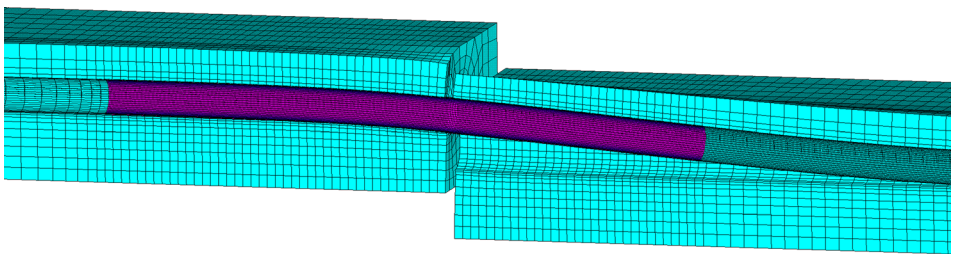

Fig. 4 Fragment of the finite-element model in the deformed state

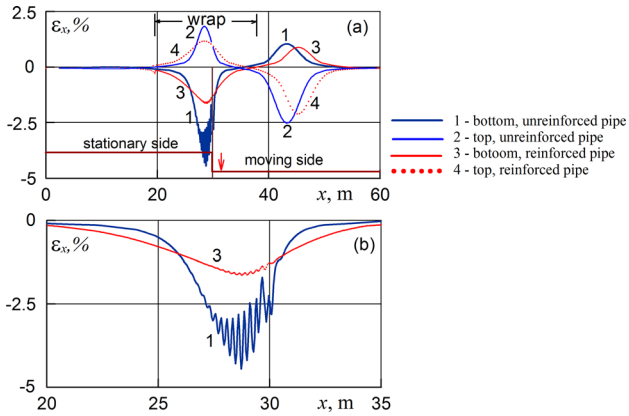

Fig. 5 (*a*) Longitudinal strain variation along the pipe under the fault offset $\Delta f = 3.0$ m. (*b*) Scaled-up view of the near-fault zone.

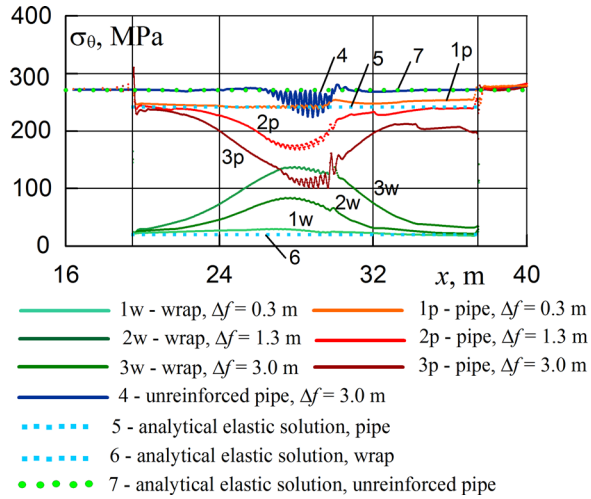

Fig. 6 Hoop stress distribution along the bottom generator in the pipe wall (*p*) and in the wrap (*w*) for the fault offset $\Delta f =$ 0.3, 1.3, and 3 m

The vertical fault displacements result in axial tension of the pipeline and bending in vertical plane. For such loading, the extreme stress and strain values are reached the top and bottom shell generators in the vertical symmetric section. Accordingly, the numerical results for stress and strain variation along the pipe are presented below for these two generatrices.

In Fig. 5(*a*), the longitudinal strain variation along the pipe is shown for the bottom (curves 1 and 3) and the top (curves 2 and 4) shell generators under the fault offset $\Delta f = 3.0$ m. Curves 1 and 2 correspond to the unreinforced pipeline; curves 3 and 4 correspond to the pipeline reinforced with a composite wrap. All results are given for the internal pipe wall surface.

As can be seen from the figure, the pipeline without reinforcement undergoes large deformations and initiation of local buckling of the pipe wall in the form of short-wave wrinkle pattern (the scaled-up view is given in Fig. 5(*b*)). Local buckling develops from the compressed side of the pipe wall (bottom generator) on the stationary side of the fault. The character of the localized buckling conforms to the experimental work on pipe bending instabilities [50] and numerical results for buried steel pipelines subjected to fault loads [17,18].

On the moving side of the fault, strains in the pipeline are lower, since the soil forces acting on this side of the fault, corresponding to the upward pipeline movement relative to the soil, are substantially lower. Maximal tensile/compressive strains attain the values 1.8%/−4.4% on the stationary side of the fault and 1.0%/−2.4% on the moving side of the fault.

Local buckling also starts to develop on the compressed side of the pipeline cross section on the moving side of the fault. Still, compared to the compressed zone on the stationary part of the fault, the intensity of the wrinkle growth and strain localization is substantially lower. This effect can be explained by a substantial difference in the magnitude of soil forces acting on the pipe in case of upward and downward pipe movement. Consequently, on the stationary side of the fault, the bending strains are more localized due to stiffer soil reaction to downward pipe movement, while on the moving side of the fault, the bending strains vary more gradually.

Curves 3 and 4, corresponding to axial strains in the pipeline strengthened with a composite wrap, display a substantial reduction in tensile and compressive strain level. The maximal effect is reached on the compressed side of the pipeline on stationary part of the fault. Maximal compressive strains reach −1.6% against −4.4% for unreinforced pipe. Maximal longitudinal tensile strains on stationary part of the fault reach the value of 1.17%, which is substantially lower than the ultimate tensile strain of the composite structure. Typical value of ultimate tensile strain ε_{1t}^u for E-glass/epoxy woven fabric composite can be assessed as 2.5–3.0% [37,41]. Compressive failure mechanisms of woven fabric composites are more complicated and include fiber crushing, microbuckling, delamination of surface layers, shear band formation, and matrix failure [51,52]. The realization of particular failure mechanism and corresponding failure stress or strain depends on a number of factors, including composite structure and geometry, loading conditions, and stress state. Based on the available data [37,51–53], an estimate for the ultimate compressive strain $\varepsilon_{1c}^u = -1.5\%$ is adopted in the present paper. Accordingly, the stress–strain state in the wrap reached under the fault offset $\Delta f = 3.0$ m can be generally characterized as critical. In Sec. 5, the allowable fault offsets are considered more closely on the basis of the pipeline and the wrap failure criteria.

As can be noted from Fig. 5(*b*), the short-wave wrinkles also begin to grow on the compressed sides of the cross section of the reinforced pipe (curve 3). Still, the strain amplitude in wrinkles is rather small. This is the earliest stage of the local buckling mechanism preceding the growth of wrinkles and the final localization of strains in one of the wrinkles. Thus, for the reinforced pipeline, development of buckling is suppressed by the stiffening action of the wrap.

It is interesting to consider the redistribution of hoop stresses between the pipe wall and the wrap on different stages of loading shown in Fig. 6. Curves 1–3 correspond to the fault offset $\Delta f = 0.3$, 1.3, and 3 m. Additional symbols "*p*" and "*w*" identify the pipe wall and the wrap. Curve 4 represents the solution for the unreinforced pipeline under the fault offset 3 m. The dashed lines illustrate the analytical solution, based on the equilibrium equation in hoop direction, plane strain assumption ($\varepsilon_x = 0$), and the Hook's law for the pipe material and the wrap

$$\sigma_\theta^s = \frac{p D_i (1-\nu_w^2) E_s}{2\left[(1-\nu_s^2) t_w E_w + (1-\nu_w^2) t_s E_s\right]} \tag{5}$$

$$\sigma_\theta^w = \frac{p D_i (1-\nu_s^2) E_w}{2\left[(1-\nu_s^2) t_w E_w + (1-\nu_w^2) t_s E_s\right]} \tag{6}$$

where σ_θ^s and σ_θ^w are the hoop stresses in the pipe wall and in the wrap (considered constant through thickness); D_i is the inner pipe diameter; and E, ν, and t are the Young's modulus, Poisson's ratio, and the wall thickness of the pipe (subscript "*s*") or the wrap (subscript *w*).

For the wrap, according to the data in Table 2, it is considered that $E_1 = E_2 = E_w$ and $\nu_{12} = \nu_{21} = \nu_w$.

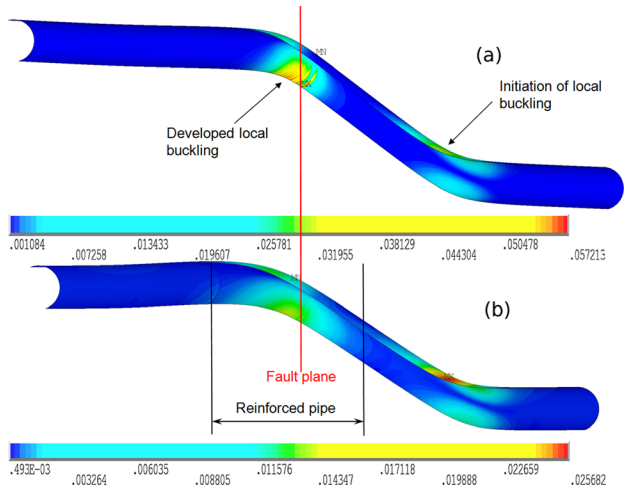

Fig. 7 Equivalent strain distributions along the unreinforced pipeline (*a*) and reinforced pipeline (*b*) under the fault offset $\Delta f = 3$ m

Also, an analytical solution based on Barlow's formula

$$\sigma_\theta = p\,D/2t_s \tag{7}$$

is given for the unreinforced pipeline with symbols.

The structure of Eqs. (5) and (6) shows that, in the elastic case, the distribution of the hoop stress between the pipe wall and the wrap is proportional to the corresponding elastic moduli. On the contrary, in case of active plastic loading, the local stiffness of the pipe material is no longer proportional to the elastic modulus of steel, but rather to the tangent modulus, which is much smaller.

As can be seen from the figure, under small fault offset, the numerical solution is close to the analytical solution. Under larger fault offsets, plastic deformations in the pipe wall in the vicinity of the fault lead to the reduction of the pipe wall stiffness and redistribution on the stresses between the pipe and the wrap. In these conditions, the role of the wrap in the load-carrying capacity of the system substantially grows.

Figure 7 illustrates the equivalent strain distributions along the unreinforced pipeline (Fig. 7(*a*)) and reinforced pipeline (Fig. 7(*b*)) under the fault offset $\Delta f = 3$ m. For the unreinforced pipeline, maximal equivalent strains are reached in the compressed zone of the shell on the stationary part of the fault. For the reinforced pipeline, the maximal equivalent strains are reached in the unreinforced part of the pipeline on the moving side of the fault. The maximal value of 2.57% corresponds to the compressed part of the shell.

5 Analysis of the Wrap Efficiency in Terms of Limit State Criteria

Verification of a pipeline design solutions at active fault crossing should be based on checking of pipeline limit state criteria for the maximal predicted fault offset. Extensive numerical modeling performed by different authors [17–20] has shown that, for the case of fault crossing at the right angle, local buckling is the most probable limit state. This limit state is controlled by the value of the maximal longitudinal compressive strains. According to Eurocode 8 [54], the critical compressive strain is calculated as min (0.01, 0.4 t/D), which gives $\varepsilon_{\rm cr}^E = -0.54\%$ for the adopted numerical values of the pipeline parameters.

The Gresnigt equation [55,56] for critical compressive strain takes into account the effect of the internal pressure

$$\varepsilon_{\rm cr} = 0.5 \cdot \left(\frac{t}{D}\right) - 0.0025 + 3000 \cdot \left(\frac{\sigma_h}{E}\right)^2 \tag{8}$$

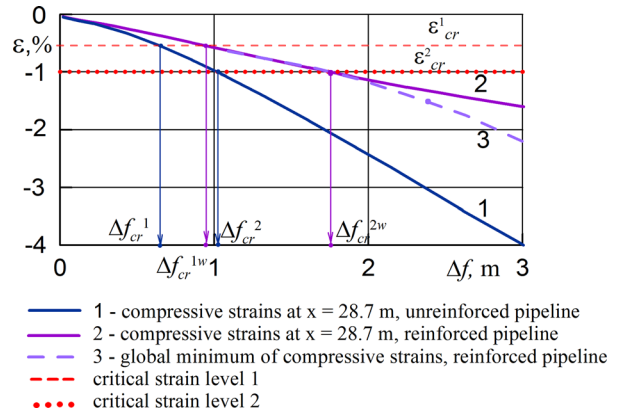

Fig. 8 Evolution of longitudinal compressive strains in the critical cross section

where the hoop stress parameter is defined as

$$\sigma_h = \begin{cases} \dfrac{pD}{2t}, & \text{if} \quad \dfrac{pD}{2t\sigma_Y} \le 0.4 \\ 0.4 \cdot \sigma_Y, & \text{if} \quad \dfrac{pD}{2t\sigma_Y} > 0.4 \end{cases} \tag{9}$$

According to Eqs. (8) and (9), the critical strain is assessed as $\varepsilon_{\rm cr} = -0.63$ %, which is slightly higher in absolute value than the Eurocode 8 estimate -0.54%.

Considering the most conservative estimate of critical compressive strains, the value $\varepsilon_{\rm cr}^E = -0.54\%$ is used as the first level of critical strain.

In the fault-crossing problem, the real critical compressive strain is larger, since the surrounding soil is an additional stiffening factor. The estimate obtained in Ref. [20] for a strike-slip fault crossing was $\varepsilon_{\rm cr} = -0.91\%$. Still, the analysis in Ref. [20] was performed for an unpressurized pipeline. Under the action of internal pressure, a buried pipeline displays a higher resistance against ovalization and local buckling.

Taking these considerations into account, two levels of critical compressive strains are adopted: $\varepsilon_{\rm cr}^1 = -0.54\%$ and $\varepsilon_{\rm cr}^2 = -1.0\%$. According to the introduced strain levels, two critical fault offsets, $\Delta f_{\rm cr}^1$ and $\Delta f_{\rm cr}^2$, can be evaluated.

It should be noted that the absolute value of critical strain characterizing possible wrap failure under compression, $\varepsilon_{\rm cr}^w = -1.5\%$, is higher than $\varepsilon_{\rm cr}^2$. Thus, under the fault offsets satisfying the condition $|\min\varepsilon_x| < |\varepsilon_{\rm cr}^2|$, the wrap failure does not occur.

Longitudinal strain evolution on the compressed side of the section $x = 28.7$ m is shown in Fig. 8. Curves 1 and 2 correspond to the unreinforced and reinforced pipelines. Curve 3 represents the global minimum of compressive strains in the reinforced pipe. For $\Delta f \le 2$ m, the minimal compressive strains are reached in the considered section. For larger fault offset, the location of minimal compressive strains moves to the compressed side of the unreinforced pipe segment on the moving side of the fault (marked with "MX" in Fig. 7(*b*)).

In Fig. 8, the introduced critical compressive strain levels are given with dashed lines. Critical fault offsets can be assessed as: $\Delta f_{\rm cr}^1 = 0.65$ m and $\Delta f_{\rm cr}^2 = 1.05$ m (for the unreinforced pipeline); $\Delta f_{\rm cr}^{1w} = 0.95$ m and $\Delta f_{\rm cr}^{2w} = 1.75$ m (for the reinforced pipeline). Thus, in terms of allowable fault offsets, the composite wrap can be regarded as an effective strengthening measure.

In Fig. 9, the influence of the wrap thickness on the critical fault offsets is studied. The thickness of the wrap changes from 5 mm to 30 mm. All other parameters of the model are fixed and correspond to the previous example ($L_{w1} = 10.5$ m and $L_{w2} = 7.5$ m).

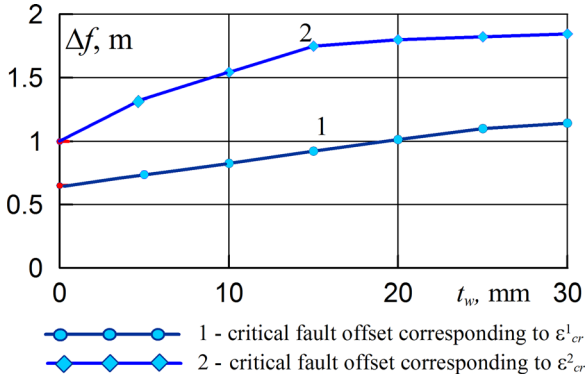

Fig. 9 Critical fault offset as a function of the wrap thickness

The critical fault offset corresponding to ε^1_{cr} changes almost linearly with the wrap thickness. This can be explained by essentially elastic behavior of the pipe before the maximal compressive strains reach the value of ε^1_{cr}.

Plastic strains are rather small, localized, and do not substantially affect the overall behavior of the pipeline. On the contrary, the critical strain level ε^2_{cr} is characterized by developed regions of plastic strains in the pipe affecting the overall structural behavior. The corresponding critical fault offset varies nonlinearly with the wrap thickness. The most essential changes in critical fault offset Δf^{2w}_{cr} take place in the range of $5 \le t_w \le 15$ mm. For higher values of t_w, the influence of thickness is rather moderate, which can be explained by strain concentration in the unreinforced pipe wall near the wrap end section on the moving part of the fault (curve 3 in Fig. 8). This effect is caused by the difference in stiffness between the unreinforced and reinforced parts of the pipeline and becomes more pronounced for higher wrap thickness. The factor of the wrap ends can be excluded by application of the wrap to a longer pipe segment exceeding in length the extensive bending zone. Thus, it can be concluded that the optimal value of the wrap thickness providing maximal strengthening effect at comparably low costs (relatively short wrap) is $t^*_w = 15$ mm. Of course, the value of t^*_w is a project-specific quantity. Different pipe geometry and loading conditions would give a different value of t^*_w.

An essential condition for an efficient application of the wrapping consists in ensuring small bending strains at the end sections of the strengthened pipeline segment. Otherwise, as will be shown below, strain concentration can develop due to abrupt stiffness change. The effect of abrupt stiffness change can also be diminished by gradual reducing of the number of the wrap plies near the ends.

The influence of the wrap length on the critical fault offsets Δf^{1w}_{cr} and Δf^{2w}_{cr} is illustrated in Fig. 10. The length $L_{w1} = 10.5$ m was fixed, while L_{w2} varied in the range of 4.5–28.5 m. Calculated

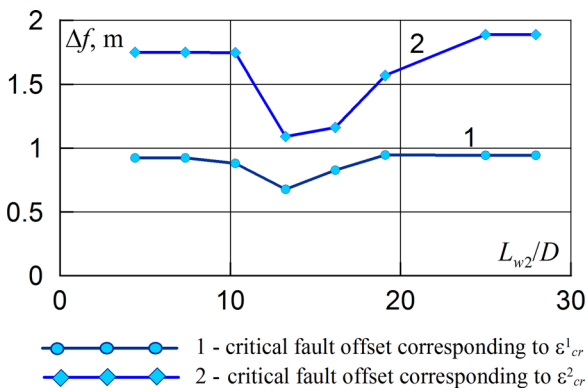

Fig. 10 Critical fault offset as a function of the wrap length

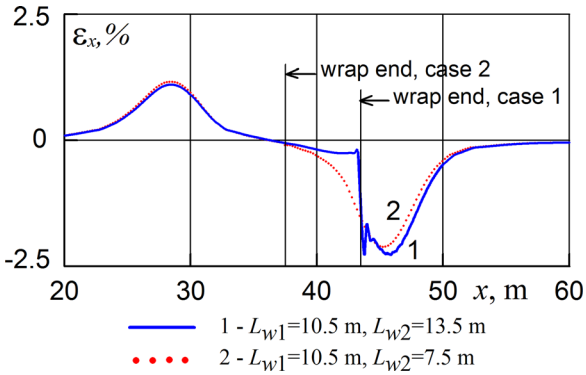

Fig. 11 Comparison of longitudinal strain distributions along the top pipe generator for the cases $L_{w2} = 13.5$ m (curve 1) and $L_{w2} = 7.5$ m (curve 2)

critical fault offsets are plotted against the nondimensional wrap length parameter L_{w2}/D. The whole range of the wrap length values can be divided into three zones. The wrap length values in the first zone $4.5D \le L_{w2} \le 10D$ cover the area of high bending strains on the stationary part of the fault. The wrap length values in the third zone $19D \le L_{w2} \le 25D$ cover the area of high bending strains on both sides of the fault. The second zone, $10D < L_{w2} < 19D$, corresponds to the wrap end section location within the area of high bending strains on the moving side of the fault. Both curves have a local minimum at $L_{w2} = 13.25D$. This value corresponds to the location of the wrap end section in the area of the maximal bending strains in the pipe wall on the moving side of the fault.

Consider this case more closely. The wrap parameters are as follows: $t_w = 15$ mm, $L_{w1} = 10.5$ m, and $L_{w2} = 13.5$ m. The longitudinal strain distribution along the top pipe generator in the near-fault zone is given in Fig. 11 (curve 1) in comparison to the cases $L_{w1} = 10.5$ m and $L_{w2} = 7.5$ m (curve 2). The curves are plotted for the fault offset $\Delta f = 3$ m.

It is seen that, in spite of longer reinforcement, the maximum value of the longitudinal compressive strains is higher, and the edge effect develops in the unreinforced part of the pipeline. Under subsequent loading, this edge effect can transform into localized buckling of the pipe wall.

For a real fault crossing, it is usually difficult to establish the exact position of the fault plane. Possible error can reach the distance of 100 m. In such circumstances, it can be recommended to apply strengthening with a composite wrap within the zone of possible surface rupture and on the length of 100 m on both sides from the bounds of this zone.

6 Conclusions

Numerical analysis of a buried steel pipeline with a composite wrap subjected to an active fault offset is performed. A three-dimensional finite-element model taking into account the geometric and material nonlinear behavior of the model is developed.

The efficiency of the application of the composite wrap for strengthening of the pipeline is analyzed on the basis of appropriate limit state criteria. It is shown that application of composite wraps on highly stressed pipeline segments in the vicinity of the fault leads to substantial reduction of stresses and strains in the pipe wall and suppresses the development of local buckling.

In the design of strengthening, positioning of the wrap ends should avoid the zones of high bending strains. Otherwise, stress and strain concentration may develop due to stiffness change between the unreinforced and reinforced pipeline segments.

The effect of geometric parameters of the wrap is studied. Allowable fault offsets are evaluated as functions of the wrap thickness and length.

Further research should be focused on the refinement of the wrap model, including contact conditions between the pipe and the wrap and modeling of the wrap failure mechanisms. Also, a study of the wrap target material properties should be conducted to reach the most efficient strengthening.

References

[1] Jennings, P. C., 1971, "Engineering Features of the San Fernando Earthquake February 9, 1971," California Institute of Technology Report, Pasadena, CA, Report No. EERL 71–02.

[2] MaCaffrey, M. A., and O'Rourke, T. D., 1983, "Buried Pipeline Response to Reverse Faulting During the 1971 San Fernando Earthquake," International Symposium on Lifeline Earthquake Engineering, 4th National Congress on Pressure Vessel and Piping Technology, Portland, OR, June 19–24, pp. 151–159.

[3] O'Rourke, T. D., and Palmer, M. C., 1996, "Earthquake Performance of Gas Transmission Pipelines," Earthquake Spectra, **12**(3), pp. 493–527.

[4] O'Rourke, M. J., and Liu, X., 1999, "Response of Buried Pipelines Subject to Earthquake Effects," Multidisciplinary Center for Earthquake Engineering Research, New York.

[5] Liang, J., and Sun, S., 2000, "Site Effects on Seismic Behaviour of Pipelines: A Review," ASME J. Pressure Vessel Technol., **122**(4), pp. 469–475.

[6] Tsai, J. S., Jou, L. D., and Lin, S. H., 2000, "Damage to Buried Water Supply Pipelines in the Chi-Chi (Taiwan) Earthquake and a Preliminary Evaluation of Seismic Resistance of Pipe Joints," J. Chin. Inst. Eng., **23**(4), pp. 395–408.

[7] Newmark, N. M., and Hall, W. J., 1975, "Pipeline Design to Resist Large Fault Displacement," U.S. National Conference on Earthquake Engineering, University of Michigan, Ann Arbor, MI, June 18–20, pp. 416–425.

[8] Kennedy, R. P., Chow, A. W., and Williamson, R. A., 1977, "Fault Movement Effects on Buried Oil Pipeline," Transp. Eng. J. ASCE, **103**, pp. 617–633.

[9] Wang, L. R. L., and Yeh, Y. A., 1985, "A Refined Seismic Analysis and Design of Buried Pipeline for Fault Movement," Earthquake Eng. Struct. Dyn., **13**(1), pp. 75–96.

[10] Karamitros, D. K., Bouckovalas, G. D., and Kouretzis, G. P., 2007, "Stress Analysis of Buried Steel Pipelines at Strike-Slip Fault Crossings," Soil Dyn. Earthquake Eng., **27**(3), pp. 200–211.

[11] Trifonov, O. V., and Cherniy, V. P., 2010, "A Semi-Analytical Approach to a Nonlinear Stress-Strain Analysis of Buried Steel Pipelines Crossing Active Faults," Soil Dyn. Earthquake Eng., **30**(11), pp. 1298–1308.

[12] American Lifelines Alliance, 2001, "Guidelines for the Design of Buried Steel Pipes," ASCE, New York.

[13] Joshi, S., Prashant, A., Deb, A., and Jain, S. K., 2011, "Analysis of Buried Pipelines Subjected to Reverse Fault Motion," Soil Dyn. Earthquake Eng., **31**(7), pp. 930–940.

[14] Trifonov, O. V., and Cherniy, V. P., 2011, "Analytical Model Versus Numerical Model in Stress-Strain Analysis of Buried Steel Pipelines Subjected to Fault Displacements," III ECCOMAS Thematic Conference on Computational Methods in Structural Dynamics and Earthquake Engineering, Corfu, Greece, May 26–28.

[15] Uckan, E., Akbas, B., Shen, J., Rou, W., Paolacci, F., and O'Rourke, M., 2015, "A Simplified Analysis Model for Determining the Seismic Response of Buried Steel Pipes at Strike-Slip Fault Crossings," Soil Dyn. Earthquake Eng., **75**, pp. 55–65.

[16] Takada, S., Hassani, N., and Fukuda, K., 2001, "A New Proposal for Simplified Design of Buried Steel Pipes Crossing Active Faults," Earthquake Eng. Struct. Dyn., **30**(8), pp. 1243–1257.

[17] Vazouras, P., Karamanos, S. A., and Dakoulas, P., 2010, "Finite Element Analysis of Buried Steel Pipelines Under Strike-Slip Fault Displacements," Soil Dyn. Earthquake Eng., **30**(11), pp. 1361–1376.

[18] Vazouras, P., Karamanos, S. A., and Dakoulas, P., 2012, "Mechanical Behavior of Buried Steel Pipes Crossing Active Strike-Slip Faults," Soil Dyn. Earthquake Eng., **41**, pp. 164–180.

[19] Trifonov, O. V., and Cherniy, V. P., 2013, "Fault Impact on Buried Steel Pipelines: Modeling and Analysis," *Advances in Engineering Research*, Vol. 7, V. M. Petrova, ed., Nova Science, New York, pp. 47–90.

[20] Trifonov, O. V., 2015, "Numerical Stress-Strain Analysis of Buried Steel Pipelines Crossing Active Strike-Slip Faults With an Emphasis on Fault Modeling Aspects," J. Pipeline Syst. Eng. Pract., **6**(1), p. 04014008.

[21] Rehberg, T., Schad, M., and Green, M., 2010, "Non-Metallic Composite Repair Systems for Pipes and Pipelines," 3R Int., **1**, pp. 42–46.

[22] ASME, 2008, "Repair of Pressure Equipment and Piping," ASME New York, Standard No. ASME PCC-2-2008.

[23] Freire, J. L. F., Vieira, R. D., Diniz, J. L. C., and Meniconi, L. C., 2007, "Effectiveness of Composite Repairs Applied to Damaged Pipeline," Exp. Tech., **31**(5), pp. 59–66.

[24] Alexander, C., and Francini, B., 2006, "State of the Art Assessment of Composite Systems Used to Repair Transmission Pipelines," ASME Paper No. IPC2006-10484.

[25] Bakis, C. E., Bank, L. C., Brown, V. L., Cosenza, E., Davalos, F., Lesko, J. J., Machida, A., Rizkalla, S., and Triantafillou, T., 2002, "Fibre-Reinforced Polymer Composites for Construction—State-of-the-Art Review," J. Compos. Constr., ASCE, **6**(2), pp. 73–87.

[26] da Costa-Mattos, H. S., Reis, J. M. L., Sampaio, R. F., and Perrut, V. A., 2009, "An Alternative Methodology to Repair Localized Corrosion Damage in Metallic Pipelines With Epoxy Resins," Mater. Des., **30**(9), pp. 3581–3591.

[27] Duell, J. M., Wilson, J. M., and Kessler, M. R., 2008, "Analysis of a Carbon Composite Overwrap Pipeline Repair System," Int. J. Pressure Vessels Piping, **85**(11), pp. 782–788.

[28] Block, N., and Kishel, J., 1995, "Clock Spring® Reinforcement of Elbow Fittings," Gas Research Institute, Des Plaines, IL, Report No. GRI-93/0346.

[29] Alexander, C. R., 2007, "Guidelines for Repairing Damaged Pipelines Using Composite Materials," NACE International Corrosion Conference and Exposition, Nashville, TN, Mar. 11–15, Paper No. 07144, pp. 349–361.

[30] Meniconi, L. C. M., Freire, J. L. F., Vieira, R. D., and Diniz, J. L. C., 2002, "Stress Analysis of Pipelines With Composite Repairs," ASME Paper No. IPC2002-27372.

[31] Ghaffari, M. A., and Hosseini-Toudeshky, H., 2013, "Fatigue Crack Propagation Analysis of Repaired Pipes With Composite Patch Under Cyclic Pressure," ASME J. Pressure Vessel Technol., **135**(3), p.031402.

[32] Trifonov, O. V., and Cherniy, V. P., 2014, "Analysis of Stress–Strain State in a Steel Pipe Strengthened With a Composite Wrap," ASME J. Pressure Vessel Technol., **136**(5), p. 051202.

[33] Reissner, E., 1945, "The Effect of Transverse Shear Deformation on the Bending of Elastic Plates," ASME J. Appl. Mech., **12**, pp. A68–77.

[34] Mindlin, R. D., 1951, "Influence of Rotatory Inertia and Shear on Flexural Motions of Isotropic, Elastic Plates," ASME J. Appl. Mech., **18**, pp. 31–38.

[35] Ramberg, W., and Osgood, W. R., 1943, "Description of Stress-Strain Curves by Three Parameters," National Advisory Committee for Aeronautics, Washington, DC, Technical Note No. 902.

[36] Crisfield, M. A., 2000, *Non-Linear Finite Element Analysis of Solids and Structures*, Vol. 2, Wiley, Chichester, UK.

[37] Daniel, I. M., and Ishai, O., 1994, *Engineering Mechanics of Composite Materials*, Oxford University Press, New York.

[38] Ishikawa, T., and Chou, T. W., 1983, "One-Dimensional Micromechanical Analysis of Woven Fabric Composites," AIAA J., **21**(12), pp. 1714–1721.

[39] Naik, N. K., and Shembekar, P. S., 1992, "Elastic Behavior of Woven Fabric Composites: I—Lamina Analysis," J. Compos. Mater., **26**(15), pp. 2196–2225.

[40] Karayaka, M., and Kurath, P., 1994, "Deformation and Failure Behavior of Woven Composite Laminates," ASME J. Eng. Mater. Technol., **116**(2), pp. 222–232.

[41] Scida, D., Aboura, Z., Benzeggagh, M. L., and Bocherens, E., 1999, "A Micromechanics Model for 3D Elasticity and Failure of Woven-Fibre Composite Materials," Compos. Sci. Technol., **59**(4), pp. 505–517.

[42] Tanov, R., and Tabiei, A., 2001, "Computationally Efficient Micromechanical Models for Woven Fabric Composite Elastic Moduli," ASME J. Appl. Mech., **68**(4), pp. 553–560.

[43] Chung, P. W., and Tamma, K. K., 1999, "Woven Fabric Composites—Developments in Engineering Bounds, Homogenization and Applications," Int. J. Numer. Methods Eng., **45**(12), pp. 1757–1790.

[44] Drucker, D. C., and Prager, W., 1952, "Soil Mechanics and Plastic Analysis or Limit Design," Q. Appl. Math., **10**(2), pp. 157–165.

[45] O'Rourke, T. D., 2010, "Geohazards and Large, Geographically Distributed Systems," Geotechnique, **60**(7), pp. 505–543.

[46] Trautmann, C. H., and O'Rourke, T. D., 1983, "Behavior of Pipe in Dry Sand Under Lateral and Uplift Loading," Geotechnical Engineering Report, Cornell University, Ithaca, NY, Report No. 83-7.

[47] Yimsiri, S., Soga, K., Yoshizaki, K., Dasari, G., and O'Rourke, T. D., 2004, "Lateral and Upward Soil–Pipeline Interactions in Sand for Deep Embedment Conditions," ASCE J. Geotech. Geoenviron. Eng., **130**(8), pp. 830–842.

[48] Davis, E. H., 1968, "Theories of Plasticity and the Failure of Soil Masses," *Soil Mechanics: Selected Topics*, I. K. Lee, ed., Butterworth, London, pp. 341–380.

[49] ANSYS, 2011, "ANSYS Release 14.0 Documentation," ANSYS Inc., Canonsburg, PA.

[50] Ju, G. T., and Kyriakides, S., 1992, "Bifurcation and Localization Instabilities in Cylindrical Shells Under Bending—II. Predictions," Int. J. Solids Struct., **29**(9), pp. 1143–1171.

[51] Fleck, N. A., Jelf, P. M., and Curtis, P. T., 1995, "Compressive Failure of Laminated and Woven Composites," J. Compos. Technol. Res., **17**(3), pp. 212–220.

[52] Malcom, A. J., Aronson, M. T., Deshpande, V. S., and Wadley, H. N. G., 2013, "Compressive Response of Glass Fiber Composite Sandwich Structures," Composites, Part A, **54**, pp. 88–97.

[53] Zhang, J., Chaisombat, K., He, S., and Wang, C. H., 2012, "Hybrid Composite Laminates Reinforced With Glass/Carbon Woven Fabrics for Lightweight Load Bearing Structures," Mater. Des., **36**, pp. 75–80.

[54] CEN EN, 2006, "Eurocode 8, Part 4: Silos, Tanks and Pipelines," Comité Européen de Normalisation, Brussels, Belgium.

[55] Gresnigt, A. M., 1986, "Plastic Design of Buried Steel Pipes in Settlement Areas," HERON, **31**(4), pp. 1–113.

[56] Gresnigt, A. M., and Karamanos, S. A., 2009, "Local Buckling Strength and Deformation Capacity of Pipes," 19th International Offshore and Polar Engineering Conference (ISOPE-2009), Osaka, Japan, June 21–26, pp. 212–223.